An Ensemble Model for Predicting the Remaining Useful Performance of Lithium-ion Batteries

Yinjiao Xing[1], Eden W. M. Ma[1], and Michael Pecht[1,2]
[1]*Centre for Prognostics and System Health Management, City University of Hong Kong, Kowloon, Hong Kong*
[2]*Center for Advanced Life Cycle Engineering (CALCE), University of Maryland, College Park, MD, 20740, USA*
yxing3@student.cityu.edu.hk[1], eden.wm.ma@cityu.edu.hk [1]
mgpecht@cityu.edu.hk[1,2]

ABSTRACT

An ensemble model is developed to characterize the capacity degradation and predict the remaining useful performance (RUP) of lithium-ion batteries. The model fuses an empirical exponential and polynomial regression model to battery degradation trends over its cycle life based on the experimental data analysis. Model parameters are adjusted online using a particle filtering (PF) approach. Experiments were conducted to compare the developed ensemble model's prediction performance with the individual results of the two empirical models mentioned above. Then, another set of experimental battery capacity data is used to validate the developed model, and the limitations of the developed model are discussed.

Key Words: Lithium-ion batteries; regression model; remaining useful performance; particle filtering; prognostics.

1. INTRODUCTION

In battery-powered systems, lithium-ion batteries are being incorporated into consumer products ranging from electric vehicles to space systems [1]. Compared with lead-acid, nickel-cadmium, and nickel-metal-hydride batteries, lithium-ion batteries offer a higher energy density, longer cycle life, and lower self-discharge rate [2, 3]. However, battery performance degrades with cycling and aging. To use the battery in an electric vehicle as an analogy, it is similar to a "fuel" tank, which shrinks with use so the driver can never know what a full or partial fuel reading actually means with respect to miles that would be achievable. Since its degradation cannot be measured directly, there is a need to estimate its maximum available performance, and tell users the accurate fuel gauge ahead of time, so that decisions for battery replacement can be made.

Remaining useful performance (RUP) is defined as the length of time from the time of prediction to the time when the predetermined end of performance (EOP) criterion is reached. In the battery community, EOP can be regarded as the failure time when the maximum available capacity reduced to 80% of its initial values, and also be determined by different manufacturers or applications [4, 5]. Since it is a pseudo failure, it is more reasonable than remaining useful life (RUL) defined in the mechanical or electronic area, although the latter has been accepted in battery research as well [6-8]. RUP indicates how much available performance the battery has left from its current status, namely state-of-health (SOH) [9, 10]. Currently, the estimation and prediction of a battery's state of charge (SOC) have been conducted and implemented in the form of the remaining time or range in today's battery management system (BMS) [11-15].However, there are few studies working on RUP prediction, which is still in the preliminary and immature stage. The first reason is that many uncertainties including the operational and environmental factors, unit-to-unit variation, and measurement noise will impose a big challenge

on the RUP prediction. Secondly, it is difficult to know the maximum releasable capacity unless the battery is fully charged and discharged in each cycle. Partial charge and discharge is usually the case in real applications. Furthermore, there still exists a great controversy on the definition of battery SOH, which is advocated considering the weighting factors, such as internal resistance, self-discharge, and cycle counting, except the loss of capacity. [1, 13, 16]. Any of marginal readings will affect the result due to the uncertainty of the weighting

Currently, the prediction of battery's RUP has been performed on the model-based and data-driven approach. Kozlowski [17] proposed a Randles circuit-based electrochemical model by electrochemical impedance spectroscopy (EIS) measurements. The internal lumped resistance was used to characterize the capacity degradation of the battery. The model parameters were extracted and fed into auto-regressive moving average (ARMA), fuzzy logic, and neural network estimator to make a fused decision on battery's SOH and RUL. Pattipati et al. [13] employed a modified Randles circuit model to characterize the model parameters, which were estimated by fitting into EIS data. The capacity fade and power fade were combined to indicate the present SOH, and to predict the RUL. Support vector regression was used to predict the pre-defined failure when arriving at a combination of 30% capacity fade and 50% power fade. Saha et al. [9] proposed the use of a relevance vector machine to study the nonlinear characteristics of the lumped parameter model based on the EIS data. Particle filtering (PF) approach was employed to track and predict the RUL with a probability density function (PDF). It can be seen that EIS measurements have been used in much research work to extract the internal parameters, which characterized various ageing and fault processes. However, online applications of the EIS technique suffer from size limitations and high cost. Moreover, it is time consuming and difficult to quantify the internal impedance at low frequency [13]. Another key problem is that the noises of an online system impact the accuracy of the EIS measurements due to a slight excitation signal required for EIS measurement. Prediction based on the empirical model was highly recommended to address these challenges in [7, 18, 19].

He et al. [7] introduced an empirical exponential model to conduct curve fitting for capacity fade data. The model parameters were initialized via Dempster-Shafer theory, which is effective to fuse varieties of battery data and apply in the parametric initialization. The parameters were updated step-by-step (each cycle) through PF. Micea et al. [18] adopted an empirical second-order polynomial model as a function of cycle number to estimate the stored maximum capacity. The proposed least square algorithm was implemented to estimate the capacity function.

In this paper, we develop an ensemble degradation model that integrates the above two regression models, the exponential and polynomial model [7, 18]. The ensemble model is a more accurate parametric model taking into account onboard applications, global and local regression characteristics. Based on the new model, the capacity degradation of the battery can be captured well and the fade trend can be tracked to implement the accurate RUP prediction. PF is used to track the aging dynamics that possess the nonlinear and non-Gaussian characteristics. The predicted results of RUP are presented with a narrow PDF. Moreover, another battery set with a different rated capacity is used to validate the performance of the developed model. The effectiveness and robustness of the developed model is proved through comparing to the other two models.

This paper is organized as follows: Section 2 compares the regression analysis of the capacity degradation based on three different models. The new model is developed based on our experimental data and comparative results. Section 3 introduces the PF approach for state estimation. Then, the framework for battery state estimation and prediction is presented in terms of integrating the regression model with PF approach. Section 4 shows the

RUP results and performance comparison according to the above framework. The developed model is then validated to demonstrate its robustness using a different battery set.

2. EMPIRICAL MODELS

2.1 Capacity measurement

Capacity denotes the amount of charge that comes out of a battery from the full to empty state corresponding to the preset upper and lower cut-off voltage by manufacturers [16]. It is calculated by integrating the current over time [20]. The SOH indication in our study is based on the maximum available capacity, which can be obtained by discharging from a full (100%) to empty charge (0%) in each cycle. Although it is impractical to fully charge or fully discharge the battery in certain applications, such as in a continuously operational uninterruptable power supply (UPS), our purpose is to exploit the degradation model for SOH estimation. In order to attain this aim, the batteries in this study went through the full charge and discharge test. The rated capacity of the tested lithium-ion battery was 1.35Ah. Using Arbin BT2000, the batteries were fully charged under a constant-current constant-voltage mode that is widely used in the industry. Then they were discharged at a 1C rate, which is 1.35A for the battery in this case. The test was run at room temperature, which was approximately 25ºC. The discharge capacity was recorded after each full charge-discharge process. The capacity fade is shown in Figure 1, while the EOP was predefined as 80% of its initial capacity.

2.2 Regression analysis based on different models

To reduce the computational complexity and consider the real application, an exponential model (model A) [7] and a polynomial model (model B) [18] were established through fitting a large amount of battery degradation data. Model A is made up of two exponential functions, while model B is a polynomial regression model.

Model A (exponential model):

$$C_{Ak} = C_{Ak1} + C_{Ak2} = \alpha_1 \cdot \exp(\alpha_2 \cdot k) + \alpha_3 \cdot \exp(\alpha_4 \cdot k) \quad (1)$$

Model B (polynomial model):

$$C_{Bk} = C_{Bk1} + C_{Bk2} + C_{Bk3} = \beta_1 k^2 + \beta_2 k + \beta_3 \quad (2)$$

where C_{Ak} and C_{Bk} are the capacity of the battery and k is the cycle number. The capacity data over the whole life (to 80% of the initial capacity) were used to evaluate the goodness-of-fit of these two parametric models.

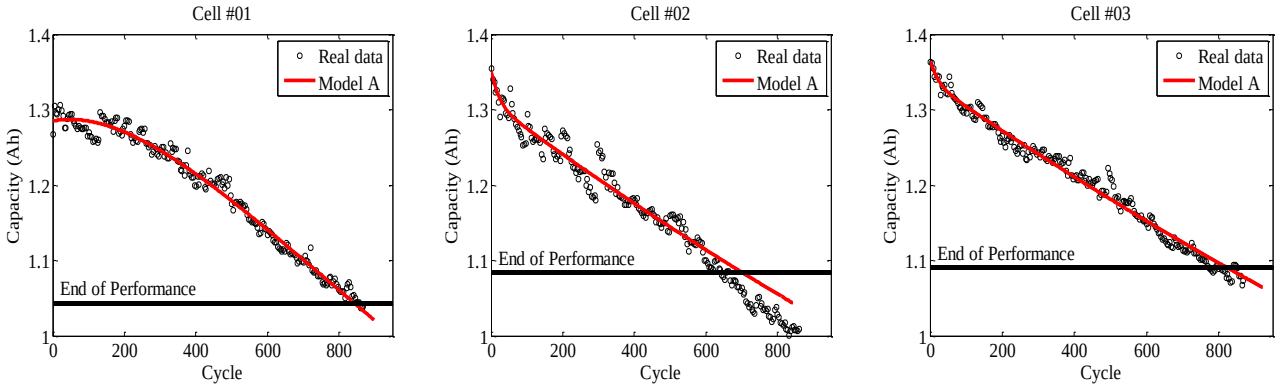

(a)

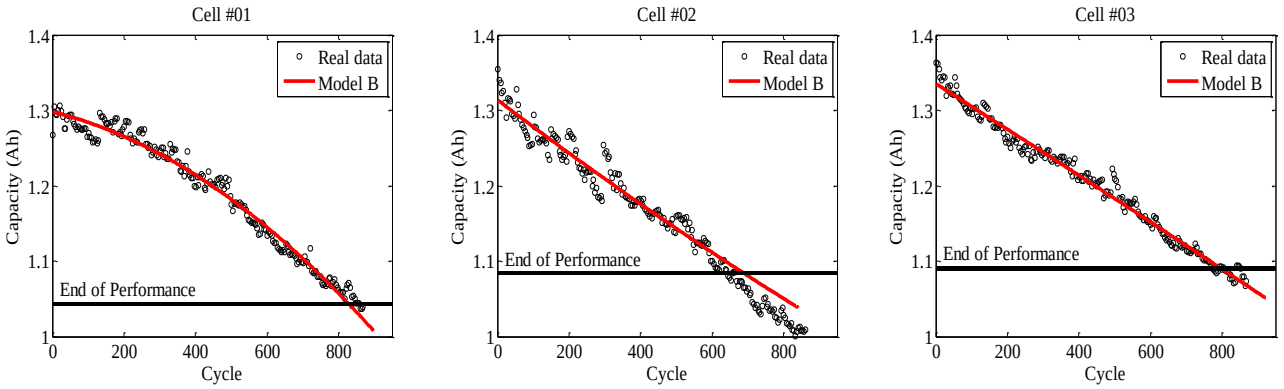

(b)

Figure 1. Curve Fitting based on (a) Model A, and (b) Model B.

Figure 1 (a) and (b) show curve fittings of models A and B, respectively. Taking Cell #01~#03 as an example above is because Cell #01~#02 presents the greater variation in the degradation process, while the small variation is shown by Cell #03 as similar as Cell #04~#06. It can also be reflected according to Table II that will be demonstrated later. The model parameters of models A and B were fitted in a MATLAB environment. With respect to the model's characteristics, model A was fitted using the nonlinear least square method, while model B was estimated by linear least square. Both criteria aim to minimize the sum of the squares of the errors [21]. The more accurate the model is, the better the prediction performance will be. The adjusted R-square (R^2_{adj}) and root mean squared error (RMSE) were two indices to compare the goodness of fit of these two models shown in Table I. The best fit is indicated by a one in R^2_{adj} and a zero in RMSE.

Table I. Goodness-of-Fit of Model A and B

No. of Cell	R^2_{adj}		RMSE	
	Model A	Model B	Model A	Model B
Cell_#01	0.9832	0.9795	0.0101	0.0112
Cell_#02	0.9497	0.9442	0.0144	0.0152
Cell_#03	0.9803	0. 9793	0.0097	0.0100
Cell_#04	0.9609	0.9517	0.0130	0.0144
Cell_#05	0.9749	0.9664	0.0101	0.0118
Cell_#06	0.9712	0.9603	0.0108	0.0127

Model A showed a better regression performance compared to model B using the whole capacity data before EOP. However, the fitting result is based on global regression that cannot characterize the local regression performance of both models. In fact, it is difficult to capture the battery aging evolution using a single model due to the changing cell characteristics. The capacity fade of lithium-ion battery could have several stages with different degradation trend. Spotnitz [5] partitioned the capacity fade into four regions according to manufacturers' information, while Zhang [22] divided the degradation into three stages based on the experimental data. However, the pattern of each fade stage is difficult to identify because of different material properties and operational

conditions. Thus, the division of different degradation stages should be determined individually. In this paper, all the capacity data before hitting the EOP are partitioned into three identical portions. Our purpose is not to distinguish different fade patterns, but to analyze the local regression characteristics of models A and B, and exploit an ensemble model that provides the potential for better fits to the whole life data. The regression results when the models are fitted in the different portions are shown in Table II.

Table II. Goodness-of-Fit of Models A and B under Different Data Portions

No. of Cell	R_{adj}^2 (The first one-third)		R_{adj}^2 (The second one-third)		R_{adj}^2 (The last one-third)	
	Model A	Model B	Model A	Model B	Model A	Model B
Cell_#01	0.2915	0.2244	0.8866	0.8852	0.9234	0.8603
Cell_#02	0.7632	0.6849	0.5153	0.5075	0.7925	0.8011
Cell_#03	0.9259	0.8669	0.6050	0.6621	0.9028	0.9354
Cell_#04	0.8824	0.8273	0.7417	0.8018	0.7302	0.5517
Cell_#05	0.8984	0.8361	0.8284	0.8698	0.6986	0.7188
Cell_#06	0.9160	0.8485	0.74266	0.7799	0.7926	0.6950

For the first third of data, larger R_{adj}^2 values were obtained from model A. However, for the second portion, model B presents a better fit for Cell_#03~#06. For the last portion, model A only has a better good-of-fitness for three of cells (i.e., Cell_#01, #04, and #06). It can be seen that model A is more suitable for tracking degradation earlier in the battery life. Thus, it offers an opportunity to develop a more accurate model, which not only has a better global regression, but also provides an accurate prediction, especially when measuring more capacity data. It is worth noting that the poor fitting results are presented for Cell_#01~#02. In Figure 1, it can be seen that there are the great dynamic changes in capacity fade. Considering the similar degradation characteristics of Cell_#03~#06, these four cells are used as test samples to establish the degradation model and training model parameters while Cell_#01 and #02 are used as the test samples in this case.

2.3 Model Selection and Validation

2.3.1 Model Selection

Since both models A and B only fit partial data well, an ensemble model is developed to fuse these two models in order to achieve a good global goodness-of-fit as well as a more accurate prediction when measuring up to the middle and late stages of degradation. A weighing factor will impose a more complex model due to the increasing number of estimated parameters. However, our purpose is to find an accurate model without introducing more parameters. Through fitting the experimental capacity data, the ensemble model (Model C) is developed as follows:

In model A, only one of the exponential parts (C_{Ak2}) plays a vital role in the regression process. Taking the training samples (Cell_#03~06) as examples, C_{Ak1} can be ignored compared to the scale of C_{Ak2} (Table III). In model B, the quadratic and linear items are compared to reduce the possible number of model parameters. Since both C_{Bk1} and C_{Bk2} refer to the variable k, the comparison is conducted among three models: C_{Ak2} +C_{Bk1} +C_{Bk3} (Model C1), C_{Ak2} +C_{Bk2}+C_{Bk3} (Model C2) and C_{Ak2} +C_{Bk1}+C_{Bk2}+C_{Bk3} (Model C3) in Table IV. When comparing regression models that use the same dependent variables and the same estimation period, the fact that

RMSE goes down is equivalent to that R_{adj}^2 goes up. Thus, R_{adj}^2 is kept to quantify the regression performance here. In addition, Akaike information criterion (AIC) is introduced to make the auxiliary assessment for model selection in order to impose a heavier penalty on model complexity.

Table III. Variation of C_{Ak1} and C_{Ak2} (Ah) over k in the Whole Life

No. of Cell	Variation of C_{Ak1}	Variation of C_{Ak2}
Cell_#03	0.0278 ~ 1.066e-17	1.336 ~ 1.104
Cell_#04	0.091 ~ 6.843e-05	1.260 ~ 1.097
Cell_#05	0.0682 ~ 2.865e-06	1.290 ~ 1.106
Cell_#06	0.0766 ~ 8.495e-06	1.279 ~ 1.106

Table IV. Comparison among Three Models

No. of Cell	C_{Ak2} +C_{Bk1} +C_{Bk3} (Model C1)		C_{Ak2} +C_{Bk2}+C_{Bk3} (Model C2)		C_{Ak2} +C_{Bk1}+C_{Bk2}+C_{Bk3} (Model C3)	
	R_{adj}^2	AIC	R_{adj}^2	AIC	R_{adj}^2	AIC
Cell_#01	0.9796	-5216	0.979	-5191	0.9797	-5217
Cell_#02	0.9525	-3659	0.951	-3639	0.953	-3663
Cell_#03	0.9863	-5246	0.9793	-4925	0.9864	-5245
Cell_#04	0.9609	-3716	0.9609	-3716	0.9609	-3714
Cell_#05	0.9747	-4081	0.9468	-3560	0.9749	-4084
Cell_#06	0.9716	-3852	0.9713	-3846	0.9717	-3851

2.3.2 Model Validation

Model accuracy and prediction performance will be validated in this section. AIC is measured to provide validation among a series of nonlinear models and is widely used for model selection to consider model complexity. It is suitable to select the preferred model as a supplement to other indicators (i.e., R_{adj}^2, RMSE) and includes a penalty for increased model complexity [23].

$$\mathrm{AIC} = 2m - 2\ln(L), \tag{3}$$

where m is the number of parameters (a penalty), and $\ln(L)$ is the maximum value of log-likelihood of the estimated model.

$$\mathrm{In(L)} = -\frac{\mathrm{N}}{2} \cdot \left[\mathrm{In}\left(2\pi \cdot \frac{\sum_{\mathrm{i}=1}^{\mathrm{N}} (\mathrm{y_i} - \hat{\mathrm{y}}_{\mathrm{pi}})^2}{\mathrm{N}}\right) + 1\right] \tag{4}$$

where N is the sample size while $y_i - \widehat{y_{pi}}$ calculates the residuals from the nonlinear least square fit. The lower the AIC is, the better the model will be [24]. In terms of the values of R_{adj}^2 and AIC in Table IV, the goodness-of-fit based on model C1 and C3 is better than that of model C2. However, AIC is not sufficient to reflect the model over-fitting that could be triggered by estimating more parameters. Therefore, the prediction performance of the model needs to be validated based on part of the capacity data. In our case, the prediction was conducted to extrapolate the estimated curve based on the fitted model, whose parameters were estimated by the nonlinear least

square approach using the first 75% of the capacity data. Model C3 could possibly reduce the training errors because of having greater complexity, but would pose a risk of over-fitting and cause a poor prediction at the same time. Figure 2 presents an over-fitting result under model C3.

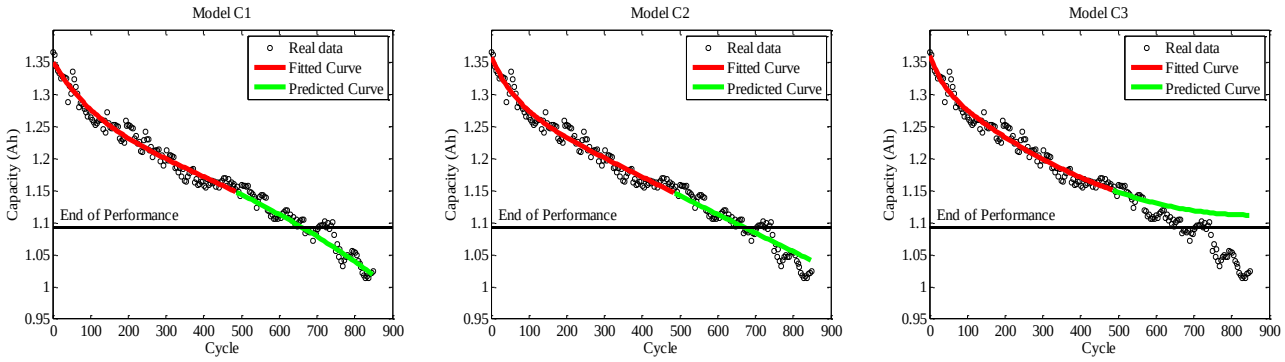

Figure 2. Prediction based on Model C1, C2 and C3 Individually under the First 75% of Capacity Data

Thus, model C1 is regarded as the ensemble model in terms of a good fitting result and predicted validation. Later, the ensemble model is known as model C below.

Model C (ensemble model):

$$C_{Ck} = \gamma_1 \cdot exp(\gamma_2 \cdot k) + \gamma_3 \cdot k^2 + \gamma_4 \tag{5}$$

3. PARTICLE FILTERING (PF) FOR RUP PREDICTION

Accurate state estimation and prediction is not only reliant on an accurate model, but also dependent on the adjustments of model parameters to track the variation of the capacity fade. In order to characterize the dynamic capacity fade, the particle filtering (PF) approach is used to estimate the current capacity. The core idea of PF is based on Bayesian Filtering and Monte Carlo simulation. Through Bayes Theorem, PF is able to provide a probability estimation for nonlinear and non-Gaussian systems [25]. In order to approximate the marginal distribution, Monte Carlo simulation is used to generate a large amount of random samples, and to estimate the posterior density function through accumulating these samples with associated weights.

3.1 Recursive Bayes

The following state-space model is fundamental to defining the tracking problem using nonlinear state, f_k, and measurement functions, h_k.

$$x_k = f_k(x_{k-1}, \vartheta_{k-1}) = \begin{bmatrix} \gamma_{1,k-1} \\ \gamma_{2,k-1} \\ \gamma_{3,k-1} \\ \gamma_{4,k-1} \end{bmatrix} + \begin{bmatrix} \vartheta_{1,k-1} \\ \vartheta_{2,k-1} \\ \vartheta_{3,k-1} \\ \vartheta_{4,k-1} \end{bmatrix} \leftrightarrow p(x_k|x_{k-1}) \tag{6}$$

$$y_k = h_k(x_k, \varphi_k) \leftrightarrow p(y_k|x_k) \tag{7}$$

where $\{x_k, k \in N\}$ is the state vector that is assumed as the unobserved Markov process. $\{y_k, k \in N\}$ are the observations or the measurements that are conditionally independent given the process. ϑ_k is an i.i.d process noise sequence, φ_k is an i.i.d measurement noise sequence, k is the time index, $p(x_k|x_{k-1})$ is the transition distribution,

and $p(y_k|x_{k-1})$ is the observation distribution. Corresponding to our case, the state x_k is the vector of model parameters $[\gamma_{1k}, \gamma_{2k}, \gamma_{3k}, \gamma_{4k}]^T$ to be estimated, while ϑ_{k-1} is distributed as $N(0, \sigma_i^2 I), i = 1,2,3,4$. y_k is the capacity sequence that is measured after a full discharge through Coulomb counting methods. Recursive Bayes provides a generic approach to estimate the posterior PDF $p(x_k|y_{1:k})$ giving the capacity and the posterior expectation $I(f_k)$ based on the sequence of measured capacity.

$$I(f_k) = \int f_k(x_k) p(x_k|y_{1:k}) dx_k \tag{8}$$

Through recursive Bayesian filtering, prediction and update will be recursively implemented in two steps. The first step is to achieve the prior PDF $p(x_k|y_{1:k-1})$, which means that the state x_k is inferred from the measurements $y_{1:k-1} = \{y_n, n = 1, \dots k-1\}$. The second is to obtain the posterior PDF $p(x_k|y_{1:k})$ in terms of the current measurement.

$$p(x_k|y_{1:k-1}) = \int p(x_k|x_{k-1}) p(x_{k-1}|y_{1:k-1}) dx_{k-1} \tag{9}$$

$$p(x_k|y_{1:k}) = \frac{p(x_k|y_{1:k-1}) p(y_k|x_k)}{p(y_k|y_{1:k-1})} \tag{10}$$

where the normalizing constant is:

$$p(y_k|y_{1:k-1}) = \int p(x_k|y_{1:k-1}) p(y_k|x_k) dx_k \tag{11}$$

where $p(y_k|x_k)$ is determined by (7).

3.2 Monte Carlo simulation for posterior PDF

Often, there is no analytical solution of equation (9) and (10), PF therefore utilizes Monte Carlo (MC) simulation to approximate the probability density with a large amount of weighed samples, which are the weighted particles. Thus, $\{x_{0:k}^i, \omega_{0:k}^i\}$ is a random measured pair that characterizes the posterior PDF, wherein, $\{\omega_{0:k}^i, i = 0, \dots, N_s\}$ is the associated weights of a set of particles $\{x_{0:k}^i, i = 0, \dots, N_s\}$, and N_s is the total number of particles. The posterior PDF at the k^{th} cycle can be approximated as:

$$p(x_k|y_{1:k}) \approx \sum_{i=1}^{N_s} \omega_k^i \delta(x_k - x_k^i) \tag{12}$$

where $\delta(\cdot)$ is a dirac function. The weights are normalized as $\sum_i \omega_k^i = 1$. The sample x_k^i is drawn from importance density $q(x_k|y_{1:k})$ based on the principle of importance sampling [26, 27]. Through recursive relation, the weights are updated as follows:

$$\omega_k^i \propto \omega_{k-1}^i \frac{p(y_k|x_k^i) p(x_k^i|x_k^{i-1})}{q(x_k^i|x_{0:k-1}^i, y_{1:k})} \tag{13}$$

Since the degeneracy of the particles will be aroused by sequential importance sampling [25], the effective sample size N_{eff} is introduced to compare with the threshold N_T. Once N_{eff} falls below N_T, the resampling will be started.

$$\widehat{N_{eff}} = \frac{1}{\sum_{i=1}^{N_s} (w_k^i)^2} \tag{14}$$

The expectation of the state can be estimated after resampling $\{x_k^i, \omega_k^i\}$

$$\widehat{I_{N_s}}(f_k) = \sum_{i=1}^{N_s} f_k(x_{0:k}^i)\, \omega_k^i \tag{15}$$

3.3 Prognostics of RUP

Prediction for the expectation and the posterior PDF $p(x_{k+j}|y_{1:k})$ of the state at the j-step ($j = 2, \dots, T-k \in N$) ahead is expected. T is the time horizon related to cycles of the battery. Since the new measurement y_{k+j} has not been collected, the present or measured state vector and its current posterior distribution $p(x_k|y_{1:k})$ would be projected among all possible future paths. Each capacity trajectory can be calculated by model C:

$$C_{k+j}^i = \gamma_{1,k}^i \cdot \exp\left(\gamma_{2,k}^i \cdot (k+j)\right) + \gamma_{3,k}^i \cdot (k+j)^2 + \gamma_{4,k}^i \tag{16}$$

While the posterior distribution of the capacity at the current cycle (cycle k) is as follows:

$$p(C_{k+j}|C_{1:k}) \approx \sum_{i=1}^{N_s} \omega_k^i \delta(C_{k+j} - C_{k+j}^i) \tag{17}$$

The expectation of posterior capacity is calculated according to (14)

$$\hat{C}_{k+j} = \sum_{i=1}^{N_s} \omega_k^i C_{k+j} \tag{18}$$

In this case, C_k represents a battery health indicator, and the RUP is the remaining time before it hits the pre-defined performance threshold, 80% of its initial capacity. For each cycle where $k+l$ projects l steps ahead of the current cycle k, the estimate $\hat{p}(RUP \geq l|C_{1:k})$ is equal to $\hat{p}(C_{k+l} \leq 0.8C_{init}|C_{1:k})$. As time proceeds, the estimate is updated with the new measurements collected $\{C_j, j = k+1, \dots, k+l\}$

The posterior PDF of RUP at cycle $k+l$ can be estimated through the transferring equation (16):

$$p(RUP_{k+l}|C_{1:k}) \approx \sum_{i=1}^{N_s} \omega_k^i \delta(RUP_{k+l} - RUP_{k+l}^i) \tag{19}$$

The expectation of RUP, according to equation (14), is:

$$\widehat{RUP_k} = \sum_{i=1}^{N_s} RUP_k^i \omega_k^i \tag{20}$$

The iteration and framework of prognostics based on PF proceeds as follows:

At cycle $k = 0$

Step 0: Initialization

- Sample $x_0^i \sim p(x_0)$, set $\omega_0^i = 1/N_s$, $i = 1, \dots, N_s$

At cycle $k \geq 1$, For $k = 1, \dots, T$

Step 1: Importance Sampling

- For $i = 1, \dots, N_s$,
  - Propagate particles: $x_k^i \sim q(x_k | x_{k-1}, y_k)$
  - Assign importance weight: $\widetilde{\omega}_k^i$ according to (13)

Step 2: Weight Calculation

- Normalize weights: $\omega_k^i = \frac{\widetilde{\omega}_k^i}{\sum_{i=1}^{N_s} (\widetilde{\omega}_k^i)}$, $i = 1, \dots, N_s$

Step 3: Resampling

IF $\widehat{N_{eff}} < N_T$

- Select N_s particle index $j_i \in \{1, N\}$ according to weights $\{\omega_{k-1}^j\}_{1 \leq j \leq N}$
- Set $\{x_{k-1}^i = x_{k-1}^j\}$, and $\omega_{k-1}^j = 1/N$, $i = 1, \dots, N_s$

Otherwise

- Set $x_{k-1}^i = x_{k-1}^j$, $i = 1, \dots, N_s$

Step 4: State Estimation

- Substitute x_k^i, ω_k^i into (16) and (18) respectively

Step 5: RUP Prediction

- Predict RUP according to (19) and (20)

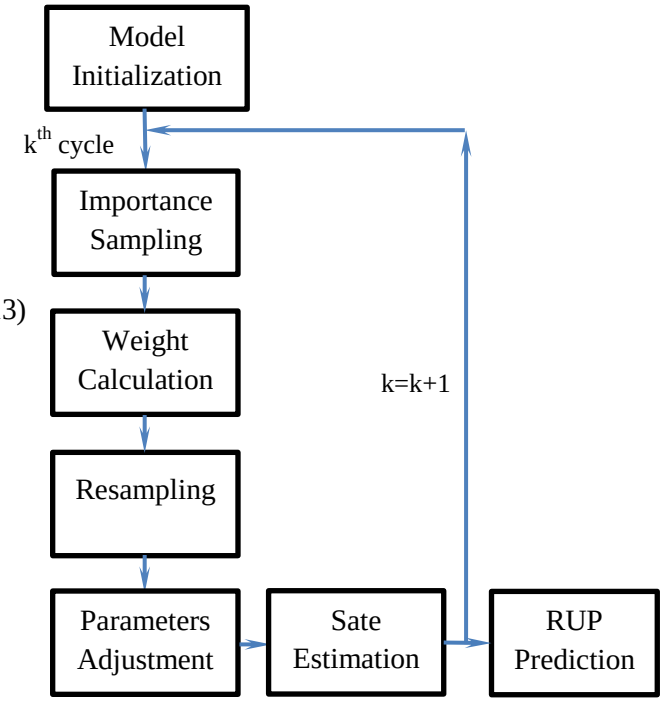

Figure 3. Flowchart of implementation of RUP Prediction

4. THE PROGNOSTIC RESULTS OF RUP

From the aforementioned description of the experiment, six battery cells were tested under the same charge mode and discharged at 1C rate. Four samples were used as the training samples to initialize model parameters, while the remaining two cells were used to test the prognostic performance due to the large fluctuation in capacity fade. A comparison was conducted among models A, B, and C, mentioned in Section 2. In addition, another battery set with a different rated capacity was tested under similar charge/discharge conditions. The objective is to validate the developed model and verify its robustness through model comparison. Similar to the previous battery set, three samples were viewed as the training samples while another one was used as a test sample.

Parameter initialization for the different models includes setting the model parameters and initial parameter variance. The model parameters are initialized using the average value of curve fitting based on battery training samples. Nonlinear least square fitting is performed to obtain the initial values of model A and C, while least square is implemented in model B throughout the whole battery life. The initialization of parameters' variance is time-consuming on the optimal setting. In order to make the prediction comparable among these three models, a similar and simple method is employed.. Taking model C as an example, the parameter vector $[\gamma_1, \gamma_2, \gamma_3, \gamma_4]^T$ is achieved according to the curve fitting for Cells_#03~#06. The variance of γ_1 can be approximated on the

assumption that the range of $[\min(\gamma_1), \max(\gamma_1)]$ is set as $6\sigma_{\gamma_1}$. This approach is also employed by the other parameters of each model, while all the initial variances $\sum_w$ of the capacity are set equal to $1e^{-05}$. Table V shows the predicted results. The prediction time K_1 is selected when cycling is conducted for up to the 1/3, 1/2, and 2/3 of the battery life. The prediction error and standard deviation (STD) are two indicators in terms of number of cycles to evaluate the prediction performance.

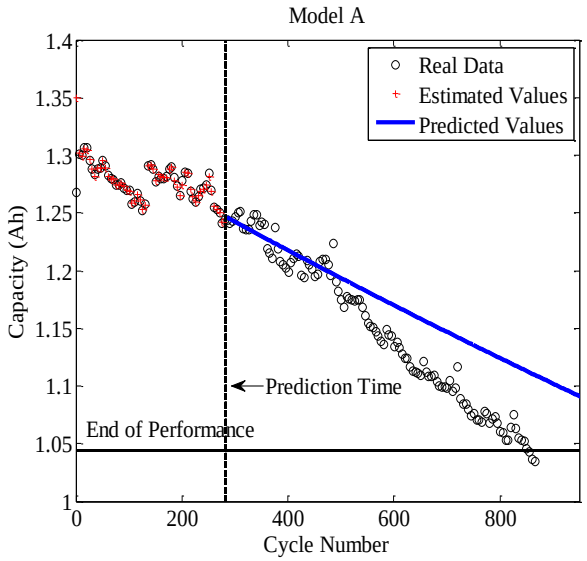

(a) Prediction result at 1/3 of life based on model A. The intersection of the projection with the EOP exceeds the length of the range of test data.

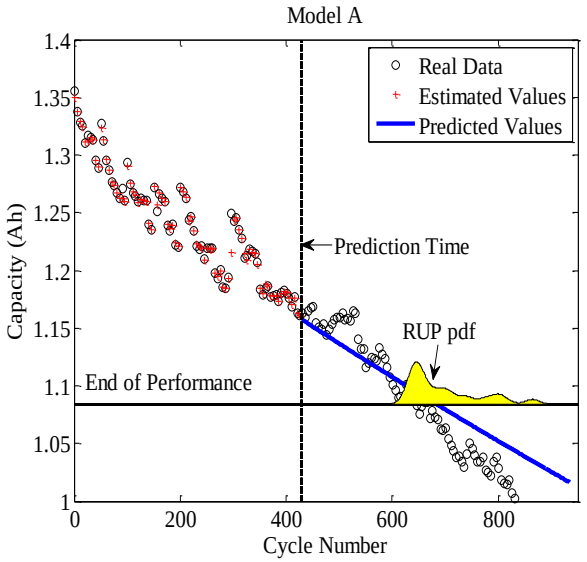

(a) Prediction result at 2/3 of life based on model B. The predicted RUP is 42 cycles later than the real one. The STD of the predicted RUP is 65.2 cycles.

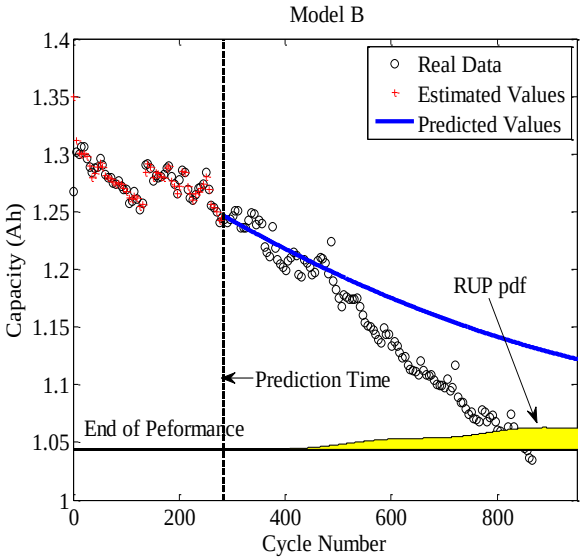

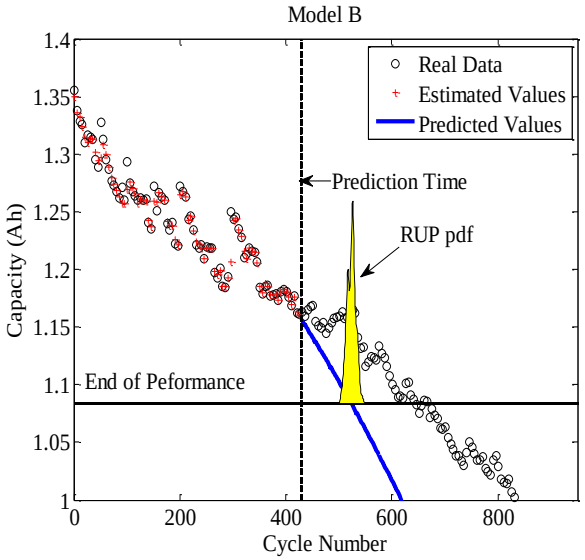

(b) Prediction result at 1/3 of life based on model B. The intersection of the projection with the EOP exceeds the length of the range of test data.

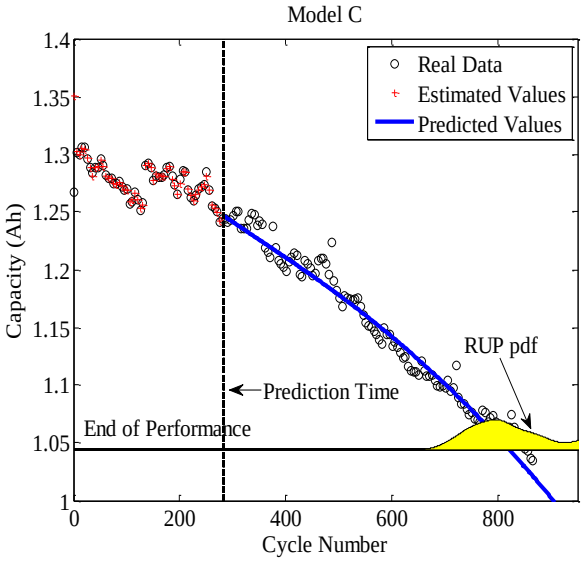

(c) Prediction result at 1/3 of life based on model C. The predicted RUP is 27 cycles earlier than the real one. The STD of the predicted RUP is 88.6 cycles.

Figure 4. Prediction Results at Cycle 283 (reaching 1/3 of life) for Cell_#01 based on Three Models

(b) Prediction result at 2/3 of life based on model B. The predicted RUP is 119 cycles earlier than the real one. The STD of the predicted RUP is 7.6 cycles.

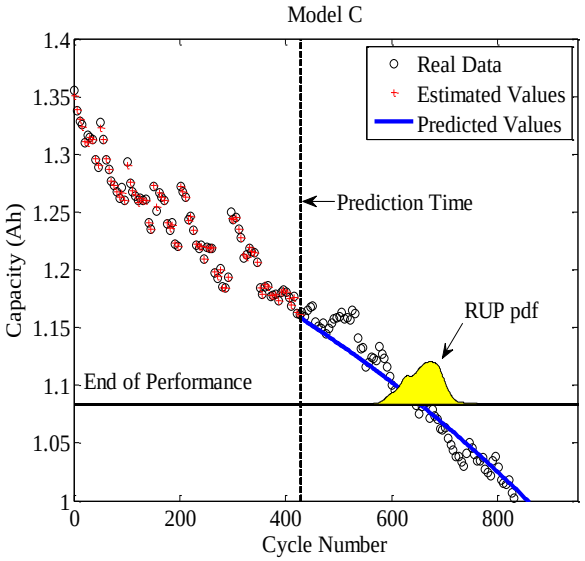

(c) Prediction result at 2/3 of life based on model C. The predicted RUP is 10 cycles later than the real one. The STD of predicted RUP is 30.7 cycles.

Figure 5. Prediction Results at Cycle 428 (reaching 2/3 of life) for Cell_#02 based on Three Models

Table V. Prediction Results for Cell_#01 and #02 at Different Cycle Numbers

	Real Failure Cycle Time	Prediction Cycle (% of life)	Model A		Model B		Model C	
			Error	STD	Error	STD	Error	STD
Cell _#01	849	283 (1/3)	325	167.6	∞(1)	284.2	-27(2)	88.6
		425 (1/2)	202	57.4	49	167	-103	46.4
		566 (2/3)	191	56.8	∞	163.3	-103	25.8
Cell _#02	643	214 (1/3)	304	50.5	-82	30.1	9	29
		322 (1/2)	133	22.8	-129	17.3	14	62.9
		428 (2/3)	42	65.2	-119	7.6	10	30.7

Note: 1) negative values mean the prediction result is earlier than the actual end of performance; 2) ∞ means that the prediction does not converge in Figure 4

In Table V, both error and STD are taken into consideration when assessing the prediction results. A small STD means narrow RUP PDF, and thus, a high confidence level for the prediction. For the assessment of the prediction result, the premise is that the actual EOP falls within the 95% confidence interval. If it were true, the smaller the absolute values of the error and STD, the more accurate the prediction. Meanwhile, a result predicted later with smaller STD should be more effective and credible than an early warning with a large STD even if the earlier result is expected. For Cell_#01, the absolute values of the prediction error and STD based on model C are

smaller than those of model A. Comparing the prediction results at1/2 of life, model B provides a smaller error than the other models, but its large STD does not make sense to the predicted result. Moreover, when predicting at1/3 of life and 2/3 of life, the projection under model B has no intersection with the EOP. For Cell_#02, predicted results are more effective and credible based on model C. Although the prediction based on model B is in advance of the time of the actual EOP, the error is so large that the real value falls outside the 95% confidence interval. Thus, model C is regarded as a better capacity degradation model to characterize the prediction performance through the parameter adjustment. By measuring more capacity data, a more accurate RUP prediction is also obtained. Taking two prediction results as examples, Figure 5 is the earlier prediction for Cell_#01 when measuring up to the first 1/3 of life (at cycle 283) while Figure 6 is the prediction for Cell_#02 when predicting at 2/3 of life (at cycle 428).

Another battery set with the rated capacity of 1.1Ah is used to validate the effectiveness and robustness of the developed model. These batteries are run in a similar test environment with the same charge-discharge mode. According to the definition of the EOP, Cell_#V1, #V2, and #V3 failed at the 469th, 472th and 434th cycles, respectively, while Cell_#V4 failed at cycle 633 because of a large dynamic change of capacity data. Thus, the first three cells are trained to average the values of the initial model parameters through fitting approaches as similar as discussed in Section 2 and #V4 is for testing. Similar to the prediction for Cell_#01 and #02, the RUP of Cell_#V4 is also predicted at different prediction cycles:1/3, 1/2, and 2/3 of capacity data.

Table VI. Prediction Results for Cell_#V4 at Different Cycle Numbers

	Real Failure Cycle Time	Prediction time (cycle K1)	Model A		Model B		Model C	
			Error	STD	Error	STD	Error	STD
Cell_#V4	633	211(1/3)	83	23.7	∞	N/A	-121	19.0
		317(1/2)	78	15.9	∞	N/A	-145	21.2
		422(2/3)	208	19.1	-80	27.7	1	83.0

Note: 1) negative values mean the prediction result is earlier than the actual end of performance; 2) ∞ means that the prediction does not converge in Figure 6

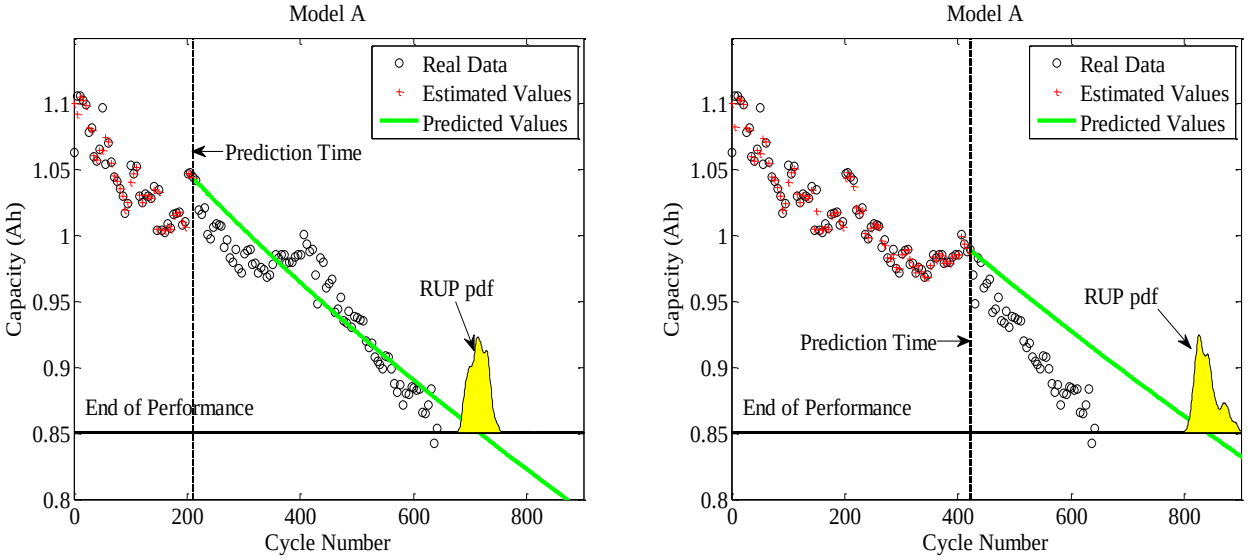

(a) Prediction result at 1/3 of life based on model A. The predicted RUP is 83 cycles later than the real one. The STD of the predicted RUP is 23.7 cycles.

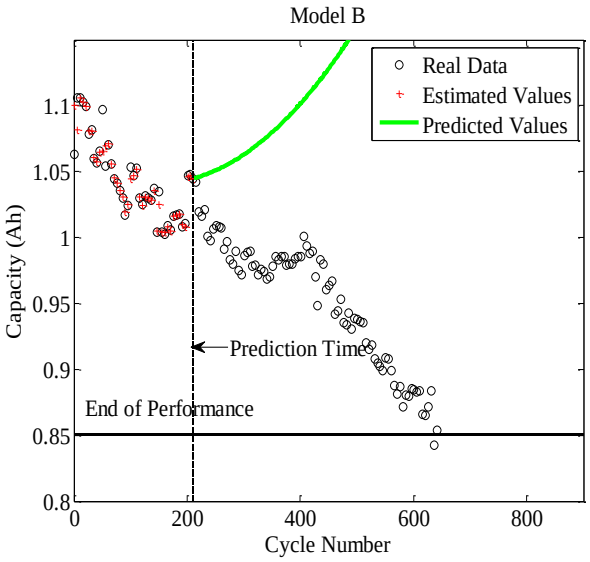

(b) Prediction result at 1/3 of life based on model B. The projection diverges, but does not converge to the EOP.

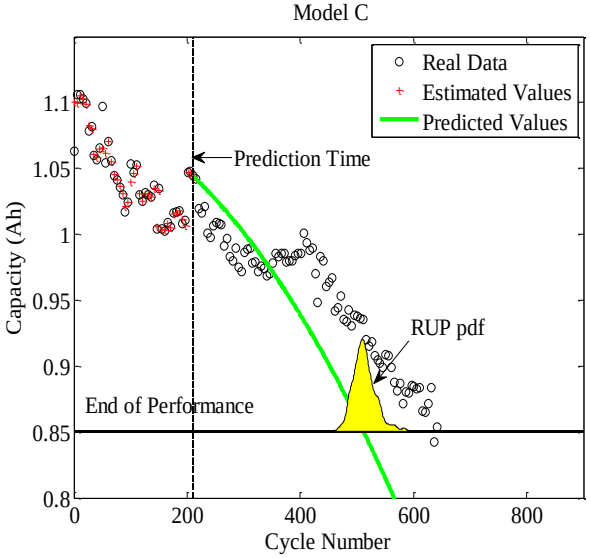

(c) Prediction result at 1/3 of life based on model C. The predicted RUP is 121 cycles earlier than the real one. The STD of the predicted RUP is 19.0 cycles.

(a) Prediction result at 2/3 of life based on model A. The predicted RUP is 208 cycles later than the real one. The STD of the predicted RUP is 19.1 cycles.

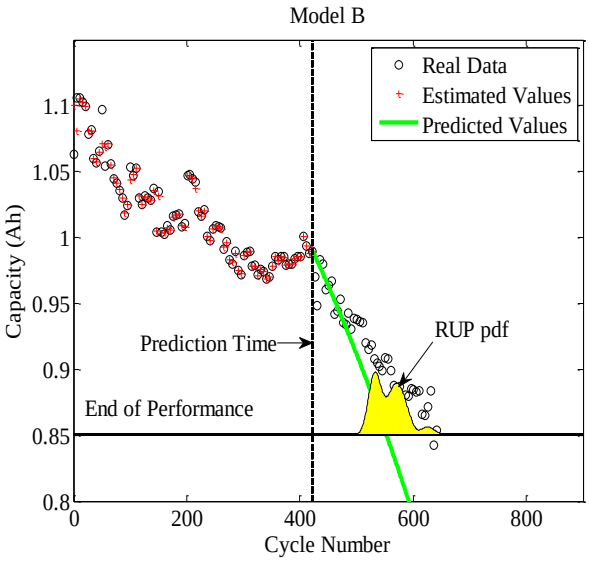

(b) Prediction result at 2/3 of life based on model B. The predicted RUP is 80 cycles earlier than the real one. The STD of the predicted RUP is 27.7 cycles.

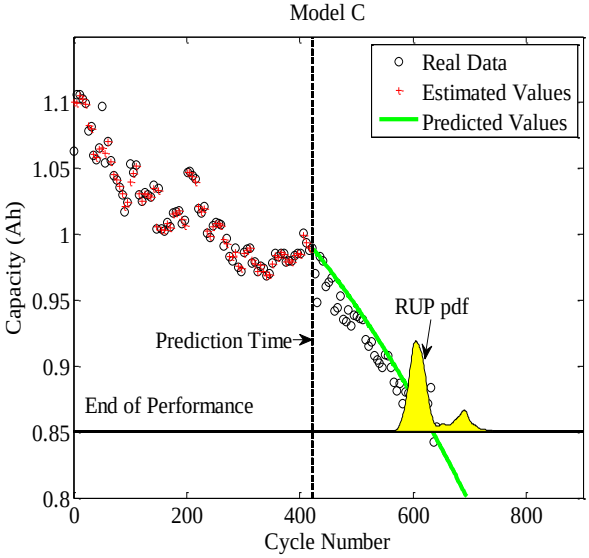

(c) Prediction result at 2/3 of life based on model C. The predicted RUP is 1 cycles later than the real one. The STD of predicted RUP is 83.0 cycles

Figure 6. Prediction Result at Cycle 211 (reaching 1/3 of life) for Cell_#V4 based on Three Models

Figure 7. Prediction Result at Cycle 422 (reaching 2/3 of life) for Cell_#V4 based on Three Models

Figures 6 and 7 show the prediction for Cell_#V4 at two different cycles. The RUP results are in line with Table VI, which indicates that model C is better to track the capacity fade of the battery than the other two models. When predicting at cycle 211 (1/3 of the capacity data), both the prediction errors are large based on model C and model A are large (Figure 6). However, an early estimated result before the actual EOP is more acceptable than comparing with a late expected value. Meanwhile, the extrapolation based on model B cannot converge to the EOP, even measuring up to 1/2 of the capacity data. In fact, the dynamic characteristics of battery aging are difficult to predict for a non-rigorous monotonically decrease. For example, there are data jumps at around cycle 210 and 420, which have a great impact on the model parameters, and therefore affect the estimated trajectory.

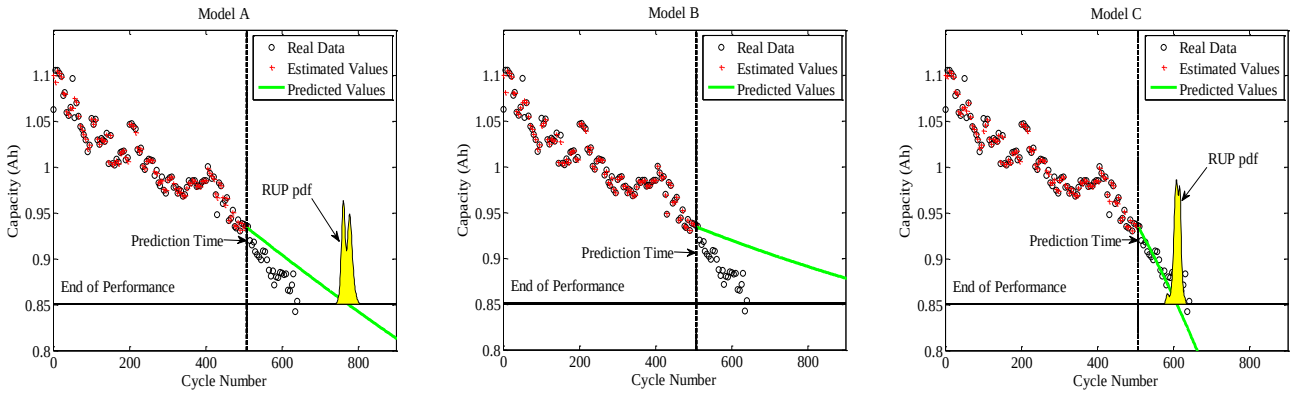

Figure 7. Prediction at the 507th Cycle (reaching 80% of life) for Cell_#V4 based on Three Models

By measuring more capacity data and adjusting the model parameters online quickly, a more accurate model is able to track the aging trend, and accordingly obtain a smaller error and a higher credibility. Figure 7 shows the predicted results when measuring up to 80% of the data (corresponding to cycle 507). The objective is to verify and compare the prediction performance in the latter stages of degradation. The estimated errors based on models A, B, and C are 141, 542, and -24 cycles, respectively. By adjusting parameters to track the changes of the aging dynamics, both models A and B cannot track the variation well compared to model C, which offers a more accurate predicted result ahead of the actual EOP with a narrower STD.

It is worth mentioning that model B's projection cannot converge to the EOP when the prediction is at cycles 211 and 317. Even if the prediction at cycle 507 converges to the EOP, the prediction is meaningless because of a large prediction error beyond the measured scope. For model B, a brief understanding is that a strong constraint should be imposed on the algebraic relationship of the model parameters to ensure a decreasing trend because of the second-order polynomial regression. However, the issue of how to use constraints to improve the prediction performance, which refer to the area related to parameter optimization, is beyond this paper's scope. Therefore, from the perspective of the degradation model, the ensemble model (model C) presents a more effective and robust characteristic for the prediction of capacity fade of the battery.

5. CONCLUSIONS

Capacity fade can be characterized as an indicator of health degradation for lithium-ion batteries. The estimation of remaining useful performance (RUP) of a battery depends on the accuracy of the degradation model. In this paper, an ensemble model, modifying from two existing empirical models, was developed to depict the capacity data that were obtained through continuous full charge and discharge cycles. It has a better regression characteristic over the whole battery life, compared with the existing empirical models. Taking into account the uncertainties in the degradation process, particle filtering was used to adjust the model parameters, and hence, calculate the estimated capacity with associated weights up to the current measured cycles. RUP was predicted by extrapolating the degradation model to EOP, while its probability distribution was approximated in terms of the associated weights bound up with the current discharge capacity.

Through comparing the predicted results from the ensemble model to the results from the exponential and polynomial models at different prediction times, the ensemble model demonstrated a better prediction performance by providing smaller prediction errors and a narrower standard deviation. Moreover, the developed model was also validated using another battery set with a different rated capacity. For these two kinds of battery samples, a credible and reliable prediction result could be achieved using a wide range of initialization and few training samples. The accurate predicted results were provided in the middle and latter stages of the prediction due to having more measured data. Thus, the developed model was demonstrated the effectiveness and robustness on the prediction of the capacity degradation.

It is meaningful to propagate the methodology that combine the degradation model with particle filtering method into other similar applications. It is worth recalling that, although an ensemble with the adjusted weights for different models is possibly better fit for the degradation, it also comes with the risk of over-fitting due to more parameters to be estimated. Hence, modification and validation for modeling is necessary using different types of battery set.

There are some unsolved problems for practical applications. In order to measure the maximum available capacity, all the battery samples were tested under the fully charged and discharged mode at a constant discharge rate. However, it is difficult to quantify the actual maximum capacity in many real life applications because it is impossible to discharge the battery to the end-of-discharge voltage for every cycle. One of the practical solutions is mapping the capacity of the partial discharge into the equivalent fully discharged capacity. The transform relation could be explored through measuring the different voltage and finding the interaction between the random cutoff discharge and fully discharged voltage. Furthermore, temperature effects on the battery degradation should also be considered in model modification and validation in future work.

REFERENCE

[1] F. Rufus, S. Lee, and A. Thakker, "Health monitoring algorithms for space application batteries," 2008, pp. 1-8.

[2] R. A. Huggins, Advanced batteries: materials science aspects: Springer Verlag, 2008.

[3] I. L. S. Kim, "A technique for estimating the state of health of lithium batteries through a dual-sliding-mode observer," Power Electronics, IEEE Transactions on, vol. 25, pp. 1013-1022, 2010.

[4] A. P. Schmidt, M. Bitzer, Á. W. Imre, and L. Guzzella, "Model-based distinction and quantification of capacity loss and rate capability fade in Li-ion batteries," Journal of Power Sources, vol. 195, pp. 7634-7638, 2010.

[5] R. Spotnitz, "Simulation of capacity fade in lithium-ion batteries," Journal of Power Sources, vol. 113, pp. 72-80, 2003.

[6] B. Saha, K. Goebel, and J. Christophersen, "Comparison of prognostic algorithms for estimating remaining useful life of batteries," Transactions of the Institute of Measurement and Control, vol. 31, pp. 293-308, 2009.
[7] W. He, N. Williard, M. Osterman, and M. Pecht, "Prognostics of lithium-ion batteries based on Dempster–Shafer theory and the Bayesian Monte Carlo method," Journal of Power Sources, vol. 196, pp. 10314-10321, 2011.
[8] B. Saha, K. Goebel, S. Poll, and J. Christophersen, "An integrated approach to battery health monitoring using bayesian regression and state estimation," 2007, pp. 646-653.
[9] B. Saha, K. Goebel, S. Poll, and J. Christophersen, "Prognostics methods for battery health monitoring using a Bayesian framework," Instrumentation and Measurement, IEEE Transactions on, vol. 58, pp. 291-296, 2009.
[10] M. Verbrugge and B. Koch, "Generalized recursive algorithm for adaptive multiparameter regression," Journal of The Electrochemical Society, vol. 153, p. A187, 2006.
[11] C. Bo, B. Zhifeng, and C. Binggang, "State of charge estimation based on evolutionary neural network," Energy Conversion and Management, vol. 49, pp. 2788-2794, 2008.
[12] S. Santhanagopalan and R. E. White, "State of charge estimation using an unscented filter for high power lithium ion cells," International Journal of Energy Research, vol. 34, pp. 152-163, 2010.
[13] B. Pattipati, C. Sankavaram, and K. Pattipati, "System Identification and Estimation Framework for Pivotal Automotive Battery Management System Characteristics," IEEE Transactions on Systems Man and Cybernetics-Part C-Applications Reviews, vol. 41, p. 869, 2011.
[14] G. L. Plett, "Extended Kalman filtering for battery management systems of LiPB-based HEV battery packs: Part 3. State and parameter estimation," Journal of Power Sources, vol. 134, pp. 277-292, 2004.
[15] Y. Xing, E. W. M. Ma, K. L. Tsui, and M. Pecht, "Battery Management Systems in Electric and Hybrid Vehicles," Energies, vol. 4, pp. 1840-1857, 2011.
[16] D. Andrea, Battery Management Systems for Large Lithium Battery Packs: Artech House Publishers, 2010.
[17] J. D. Kozlowski, "Electrochemical cell prognostics using online impedance measurements and model-based data fusion techniques," 2003, pp. 3257-3270.
[18] M. V. Micea, L. Ungurean, G. N. Cârstoiu, and V. Groza, "Online State-of-Health Assessment for Battery Management Systems," Instrumentation and Measurement, IEEE Transactions on, vol. 60, pp. 1997-2006, 2011.
[19] H. J. Bergveld, W. S. Kruijt, and P. H. L. Notten, Battery management systems: design by modelling vol. 1: Springer, 2002.
[20] J. Zhang and J. Lee, "A review on prognostics and health monitoring of Li-ion battery," Journal of Power Sources, vol. 196, pp. 6007-6014, 2011.
[21] J. Friedman, T. Hastie, and R. Tibshirani, The elements of statistical learning vol. 1: Springer Series in Statistics, 2001.
[22] Q. Zhang and R. E. White, "Capacity fade analysis of a lithium ion cell," Journal of Power Sources, vol. 179, pp. 793-798, 2008.
[23] J. Friedman, T. Hastie, and R. Tibshirani, "The Elements of Statistical Learning," ed: Spinger, 2008.
[24] A. N. Spiess and N. Neumeyer, "An evaluation of R2 as an inadequate measure for nonlinear models in pharmacological and biochemical research: a Monte Carlo approach," BMC pharmacology, vol. 10, p. 6, 2010.
[25] M. S. Arulampalam, S. Maskell, N. Gordon, and T. Clapp, "A tutorial on particle filters for online nonlinear/non-Gaussian Bayesian tracking," Signal Processing, IEEE Transactions on, vol. 50, pp. 174-188, 2002.
[26] A. Doucet, S. Godsill, and C. Andrieu, "On sequential Monte Carlo sampling methods for Bayesian filtering," Statistics and computing, vol. 10, pp. 197-208, 2000.
[27] D. J. Lee, "Nonlinear Bayesian filtering with applications to estimation and navigation," Texas A&M University, 2005.